Direct Measurement of the Flip-Flop Rate of Electron Spins in the Solid State

Ekaterina Dikarov, Oleg Zgadzai, Yaron Artzi, and Aharon Blank*

Schulich Faculty of Chemistry, Technion-Israel Institute of Technology, Haifa 3200003, Israel

(Received 30 June 2016; revised manuscript received 11 September 2016; published 3 October 2016)

Electron spins in solids have a central role in many current and future spin-based devices, ranging from sensitive sensors to quantum computers. Many of these apparatuses rely on the formation of well-defined spin structures (e.g., a 2D array) with controlled and well-characterized spin-spin interactions. While being essential for device operation, these interactions can also result in undesirable effects, such as decoherence. Arguably, the most important pure quantum interaction that causes decoherence is known as the "flip-flop" process, where two interacting spins interchange their quantum state. Currently, for electron spins, the rate of this process can only be estimated theoretically, or measured indirectly, under limiting assumptions and approximations, via spin-relaxation data. This work experimentally demonstrates how the flip-flop rate can be directly and accurately measured by examining spin-diffusion processes in the solid state for physically fixed spins. Under such terms, diffusion can occur only through this flip-flop-mediated quantum-state exchange and not via actual spatial motion. Our approach is implemented on two types of samples, phosphorus-doped ^{28}Si and nitrogen vacancies in diamond, both of which are significantly relevant to quantum sensors and information processing. However, while the results for the former sample are conclusive and reveal a flip-flop rate of approximately 12.3 Hz, for the latter sample only an upper limit of approximately 0.2 Hz for this rate can be estimated.

DOI: 10.1103/PhysRevApplied.6.044001

I. INTRODUCTION

Spin-based quantum devices, such as magnetic-field sensors [1,2] and quantum computers (QCs) [3], are potentially very useful, but they are also prone to errors and subject to limitations due to unavoidable interactions with neighboring spins and the surrounding environment. Such interactions may affect the purity and stability of a given quantum state for any electron spin in the device. Evidently, it is important to characterize these interactions and their effects on spin coherence for a variety of materials and spin arrangements (e.g., a 2D array of spins [4–8]). If we examine a typical system of electron spins in solids, we can identify several potential pure spin-related mechanisms for decoherence that can be measured by electron-spin-resonance (ESR) spectroscopy, as described in Fig. 1.

In order to properly design and optimize a specific spin-based quantum device or a sensor, it is highly important that the coherence properties of the electron spins are well understood and characterized for each and every mechanism independently. At present, the rate of this process can only be estimated theoretically [10–14], or measured indirectly, under limiting assumptions and approximations, via spin-relaxation data [15]. The problem is that in most, if not all settings, it is not possible to obtain a direct independent measurement of each and every decoherence mechanism separately. This is because coherence time is often evaluated as a single collective parameter, based on the ESR signal decay time profile as measured by spin echo [Fig. 1(g)] or a Carr-Purcell-Meiboom-Gill sequence [16,17], which eliminates only the static field inhomogeneity contribution to the decoherence and maintains all other contributions. Previous efforts to try and disentangle the various decoherence mechanisms out of the spin-echo decay data relied on the use of several sets of samples, measured under several sets of experimental conditions. A good example of such an effort was carried out recently by Lyon's team, which looked into the details of the coherence time of P-doped Si [15]. The contribution from instantaneous diffusion to decoherence is estimated by plotting the inverse relaxation time $(1/T_2)$ as a function of the second pulse rotation angle θ [$\sin^2(\theta/2)$ to be more exact] and extrapolating to $\theta \to 0$. This leads to what is referred to as the "intrinsic" T_2 of the system, T_2^{INT}, without the artificial effects of static field inhomogeneity and microwave (MW) pulses. The contribution of the ac magnetic-field noise due to nuclear spin random flips to the electron decoherence is evaluated by comparing the relaxation times of different samples with different ^{29}Si concentrations (as theoretically described in Ref. [18]) at different temperatures. The contribution from direct and indirect flip flops is estimated using a combination of measurements with different rotation angles θ carried out in either homogenous or inhomogeneous static fields (which can suppress some of the flips flops, at least along the gradient direction). This later procedure has to make some significant simplifying assumptions in order to finally extract the direct flip-flop contribution to decoherence $(1/T_2^{\mathrm{DFF}})$. Namely, it must assume a

*Corresponding author.
ab359@tx.technion.ac.il

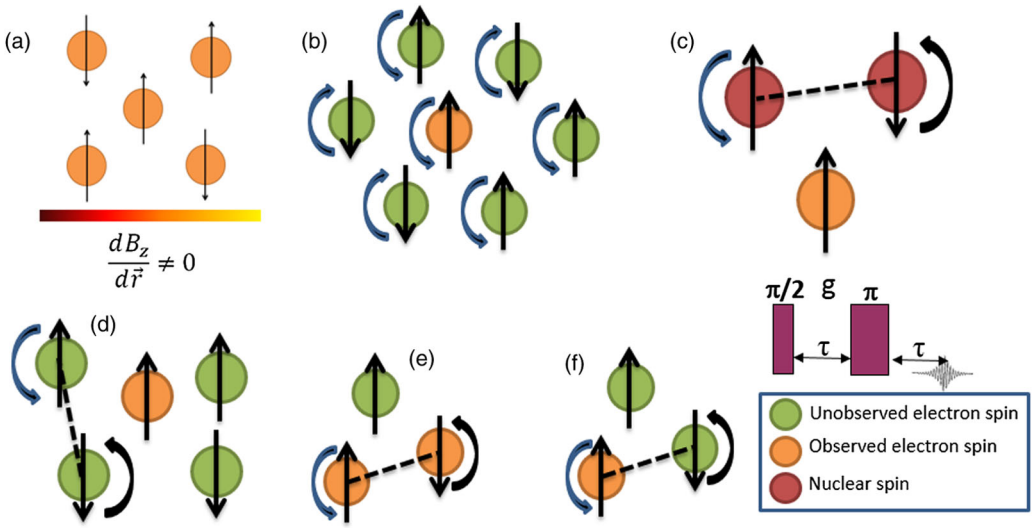

FIG. 1. Electron spin decoherence mechanisms in a solid-state sample. (a) Static field inhomogeneity leads to spatial variations in the sample's Zeeman frequencies, resulting in an extra broadening of the inhomogeneous ESR spectrum of the order of $1/T_2^{DC}$. (b) Instantaneous diffusion decoherence effects can be seen in a Hahn spin echo experiment (see item g), where the second π pulse flips not only the observed spin but also the neighboring random-state spins. This results in a stochastic change of the local magnetic fields felt by the observed spin and leads to "instantaneous" changes in its precession frequency, thus resulting in less efficient echo refocusing and shorter observed phase-memory time with an excess rate characterized by $1/T_2^{ID}$. (c) ac magnetic-field noise due to flip flops of nearby dipolar nuclear spin pairs acting on the observed electronic spin in the form of fluctuating fields and resulting in enhanced relaxation rates of the order of $1/T_2^{AC}$. Using isotopically pure samples with no magnetic nuclei reduces this decoherence effect. (d) Indirect electron-spin flip flops involve a mutual change in the quantum state of dipolar electron pairs neighboring the observed spin, which thus produce fluctuating magnetic fields shifting the observed frequency in a time-dependent manner (also denoted as spectral diffusion), with a rate given by $1/T_2^{IDFF}$. (e),(f) The direct flip-flop process, also known as spin diffusion, contributes to the overall relaxation by a rate given by $1/T_2^{DFF}$ and involves the direct exchange of polarization between the observed spin and its neighbor. This may occur between two observable spins (e), or one observable and another, unobserved spin (f). The term "observable" relates here to a spin that is excited by the microwave pulses in the spin-detection sequence. Only the former case is of relevance to decoherence [9].

simple exponential dependence of the echo amplitude on T_2^{DFF}, T_2^{IDFF}, and T_2^{ID} to extract them all from the relaxation data curve (for example, with an exponential rate of $(1/T_2) = \sin^2(\theta_2/2)[(1/T_2^{ID}) + (1/T_2^{DFF})] + (1/T_2^{IDFF})$; see Ref. [15]). This may be an oversimplification (the theory predicts a much more complex decay behavior [9]) and may potentially work only if all relaxation rates are of comparable magnitude. Unfortunately, in most samples of relevance to QCs, such as P-doped Si or nitrogen vacancies (NV) centers in diamonds, the direct flip-flop rate (and its contribution to decoherence) is very small compared to other mechanisms described above and is also almost inseparable from the indirect flip-flop effects. Moreover, additional experimental issues, such as the electromagnet's random magnetic-field noise and imperfections and inhomogeneity of the excitation MW pulses, add to the experimental complexity. Thus, the process of disentangling the direct flip-flop rate based on echo measurements' decay data may be prone to significant errors and not satisfactory, especially when longer and longer decoherence times are involved.

In the present work, we demonstrate an approach to selectively extracting and measuring the flip-flop rate of electron spins in solids, without the effort of disentangling contributions from other decoherence mechanisms. This is achieved by directly measuring the spin-diffusion process of *physically fixed spins*, where the wave function of the spins diffuses only through this flip-flop-mediated quantum-state exchange and not via actual spatial motion. Consequently, these spin-diffusion data immediately provide the flip-flop rate. Our approach is implemented on two types of samples: phosphorus-doped ^{28}Si and NVs in diamonds, both of significant relevance to quantum sensors and information processing [3,19,20]. However, while the results for the former sample are conclusive, the latter sample yields only an estimate of the upper limit of the flip-flop rate.

II. THEORY OF SPIN FLIP FLOP AND SPIN DIFFUSION

A. Spin diffusion and the flip-flop rate

The concept of the spin self-diffusion coefficient D_s was introduced a long time ago by Bloembergen, who linked it to the flip-flop rate W in his seminal paper [10]. This direct

link between W and D_s leads to the possibility of providing accurate measurements of W by measuring D_s. We can describe this relation in quantitative terms using the approach of Bloembergen [10] and those who followed his work. We assume that the $S = 1/2$ spins in the sample are located on a cubic lattice with equal spacing a and have an equal nearest-neighbor flip-flop rate $W = W_{ij}$ between spins i and j. We denote the polarization $p(x,t) = P_+(x,t) - P_-(x,t)$, where $P_{+(-)}(x,t)$ is the probability of finding at x and at time t a $|+1/2\rangle(|-1/2\rangle)$ state. Thus, based on the definition of W, it is possible to write that

$$\begin{aligned}\frac{-\partial p(x,t)}{\partial t} = W\{&P_+(x+a,t)P_-(x,t)\\ &- P_+(x,t)P_-(x-a,t)\\ &+ P_+(x-a,t)P_-(x,t)\\ &- P_+(x,t)P_-(x+a,t)\}.\end{aligned} \tag{1}$$

Using the relation $P_+(x,t) + P_-(x,t) = 1$ and neglecting terms that are quadratic in p results in the well-known diffusion equation

$$\frac{-\partial p(x,t)}{\partial t} = D_s \frac{\partial^2 p}{\partial x^2}; \qquad D_s = Wa^2. \tag{2}$$

Therefore, by measuring D_s we obtain direct knowledge about the flip-flop rate, assuming that the interspin distance a is known.

In cases where the interspin distance is not constant, as in most electron-spin samples of interest, it is possible to make use of numerical derivation of the spin-diffusion phenomenon as mediated by flip-flop processes. In the next section, we outline the details of such a numerical simulation, carried out in conjunction with our measurement protocol, which takes into account possible deviations from the average distance a and considers the interactions from all neighboring spins and also the orientation of the static magnetic field with respect to the spins.

B. Theoretical approach to calculating W

Most of the theory for calculating W was developed in the context of condensed-phase nuclear magnetic resonance (NMR), where the dipolar interaction between the spins is the dominant transverse relaxation process (T_2). While this is not the case for the electron spins in our samples, it is worthwhile to briefly describe the existing theory, as we make use of its results as a rough estimation of the expected experimental outcomes.

We consider first a system of identical spins in a solid that interact via the dipole interaction. Such a system can be described using the Hamiltonian [10,13]

$$H = H_z + H_d \tag{3}$$

with the Zeeman interaction

$$H_z = \sum_k \gamma_k B_0 \mathbf{S}_k \tag{4}$$

and the dipolar term

$$H_d = \sum_{j,k;j<k} \frac{\mu_0}{4\pi}\frac{\hbar\gamma_j\gamma_k}{r_{jk}^3}\left[\mathbf{S}_j\cdot\mathbf{S}_k - \frac{3(\mathbf{S}_j\cdot\mathbf{r}_{ij})(\mathbf{S}_k\cdot\mathbf{r}_{ij})}{r_{jk}^2}\right], \tag{5}$$

where r_{jk} is the distance between spins j and k, $\mathbf{S}_j$ is the angular-momentum operator of spin j, in $\hbar$ units, and γ_j is the gyromagnetic ratio of spin j. The dipolar interaction can be divided into several complementary terms:

$$H_d = \frac{\mu_0}{4\pi}\frac{\hbar\gamma_j\gamma_k}{r_{jk}^3}(A + B + C + D + E + F), \tag{6}$$

where each of the terms is involved in a different change of the spins' m_s quantum number. The only relevant term that induces the flip-flop process is the one where the total quantum number m_s of the two interacting spins does not change (zero quantum transition):

$$B = -\frac{1}{4}(S_j^+ S_k^- + S_j^- S_k^+)(1 - 3\cos^2\theta_{jk}), \tag{7}$$

where S_j^+ and S_j^- are the raising and lowering spin operators of spin j, respectively, and θ_{jk} is the angle between r_{jk} and the direction of B_0. Based on this description, the flip-flop rate W_{jk} can in essence be calculated from first principles, assuming that the dipole interaction is a small perturbation to the Hamiltonian [10,12–14]:

$$W_{jk} = \frac{\pi}{2}\left[\frac{\mu_0}{4\pi}\frac{\hbar\gamma_j\gamma_k}{r_{jk}^3}\right]^2\left[\frac{3\cos^2\theta_{jk}-1}{2}\right]^2 f_{jk}(0). \tag{8}$$

However, such calculations are limited by nature, since they require *a priori* data about the zero-quantum transition normalized spectral line shape function on the two-spin system, $f_{jk}(\omega)$. This line shape may be very different than the one measured for the conventional single-quantum transition spectrum, as it is much less affected by the decoherence mechanisms listed above (e.g., static field spatial inhomogeneities and temporal instabilities), and calculating it would require many details about the spatial and spectral distribution of fluctuating lattice motions and magnetic fields in the solid, which are difficult to obtain. Under the assumption that f has the same line shape as the one measured for the single-quantum transitions (assumed here to be Gaussian) and that the line-shape-broadening mechanism is mainly due to the dipolar interaction between the spins, it is possible to obtain this approximate formula

for the exchange rate between like spins randomly distributed in the solid [10]:

$$W \approx \frac{\sqrt{2\pi}}{30 T_2^{\mathrm{INT}}}, \tag{9}$$

with the notation of T_2^{INT} as referred to in the main text. However, as noted above, this formula is very approximate, especially for weakly interacting spins (where line-shape broadening is certainly due not only to the dipolar interaction) and thus can serve only as a rough order-of-magnitude estimation. Thus, while many theoretical papers can be found on the subject (mainly in the context of NMR) that are based on a perturbative approach, make use of a more rigorous density-matrix formulation [21], or even rest on a classical numerical simulation [22], in practical terms it is necessary to resort to experiments to obtain W, and, as noted above, deriving W from the decoherence rate is very problematic.

III. MEASUREMENTS OF SPIN DIFFUSION

The spin diffusion considered in this work is certainly related to, but should not be mistaken for, *real-space diffusion*, which can be more easily measured. For example, real-space diffusion of proton spins can be accurately measured by employing NMR in the presence of a static or pulsed magnetic-field gradient. In a sample with diffusing species, e.g., molecules in liquids, this leads to a significant reduction in the echo signal's magnitude, which can be directly linked to the diffusion coefficient of the spins [17,23–25]. Measuring the *diffusion of the spins' wave function* resulting from the flip-flop mechanism, when the spins are *physically fixed* in a solid, is far less common. However, there are some unique examples of just such measurements but only in the field of condensed-phase NMR, where spin-spin interactions (dipolar- or exchange-based) are relatively large with respect to the spin-lattice relaxation times that are relatively very long [26–29]. In the case of electron spins, the measurement of self-diffusion, both in real space and certainly for physically fixed spins, is far less common. The reason for that lies in the technical difficulties that arise due to the short relaxation times of the electron spins, which in turn pose extreme challenges on the required magnitude and duration of the applied magnetic-field gradients.

In order to better clarify the exact nature of our present measurements in comparison to other related electron- and electron-spin-diffusion experiments, we provide the following discussion with reference to Fig. 2. *Physical real-space diffusion* [Fig. 2(a)] was measured in the past in the unique case of conduction electrons in solids, thanks to their relatively large diffusion coefficient of $D_s > 10^{-6}$ m^2/s [30]. More recently, a much more advanced setup using a unique set including a miniature resonator and gradient coils, driven by powerful and fast gradient drivers, was employed to measure physical electron spin diffusion in liquids, with D_s as low as 10^{-10} m^2/s [31–33]. Other works, from the field of spintronics, refer to "spin diffusion length (or time)" [Fig. 2(b)] as the distance (or time) over which a nonequilibrium flow of spin population can propagate prior to decaying to thermal equilibrium

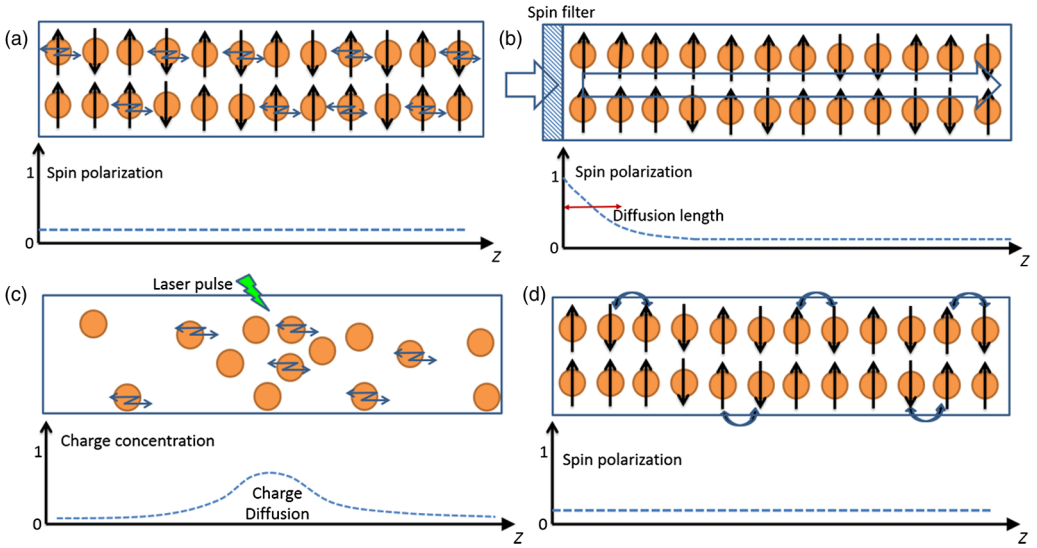

FIG. 2. Description of various electron- and electron-spin-diffusion processes and related experiments. (a) The electron spins are in thermal polarization and physically self-diffuse in a liquid (in the case of paramagnetic molecules) or in a solid (in the case of conduction electrons). (b) In spintronics, electron spins are injected to a conductor or a semiconductor through a spin "filter" resulting in a polarized electron spin current with a polarization level that decays during the "diffusion length" of the spins. (c) The electron (and not necessarily electron spin) diffusion can be measured by generating a local electron population and observing their physical diffusion. (d) Spin diffusion in physically fixed spins mediated by flip flops, as measured in the present experiments.

polarization [34]. Data on this process can be measured by advanced methods, such as muon spin rotation and Kerr-rotation microscopy [35,36]. Additional experiments of relevance observe the physical diffusion of the electrons or electron-hole pairs, without specifically considering their spin properties [Fig. 2(c)] [37,38]. As noted above, contrary to the processes described in Figs. 2(a)–2(c), our present work considers the spin diffusion of physically fixed electron spins in solids [Fig. 2(d)]. While this process is undistinguishable from that occurring in physically free spins [Fig. 2(a)], the former process can be safely neglected in insulating samples or other similar samples where electrons are not mobile. Up until now, no experiment has attempted or shown a capability to measure the diffusion of the electron spins' wave function in solids (due to flip flops), which is expected to be of the order of 10^{-15}–10^{-13} m^2/s (see below). Here we provide an account of such an experiment, which assesses the electron spins' self-diffusion coefficient and uses this measurement to provide directly the flip-flop rate for spins in a P-doped single crystal of ^{28}Si and attempts the same for NV centers in diamonds. Both of these samples are of significant relevance to quantum sensors and information processing [19,20].

The assessment of D_s in our work is carried out employing the pulsed gradient spin echo sequence (PGSE) shown in Fig. 3. The magnitude of the echo signal acquired via this sequence is given by [40]

$$E^g_{(t=2\tau_2+\tau_1)} = A\exp[-2\tau_2/T_2 - \tau_1/T_1 - D_s\gamma^2 g^2\delta^2(\Delta-\delta/3)]. \quad (10)$$

Let us first investigate, in quantitative terms, what would be the experimental requirements needed to measure D_s for a typical sample, such as P-doped ^{28}Si. The order of

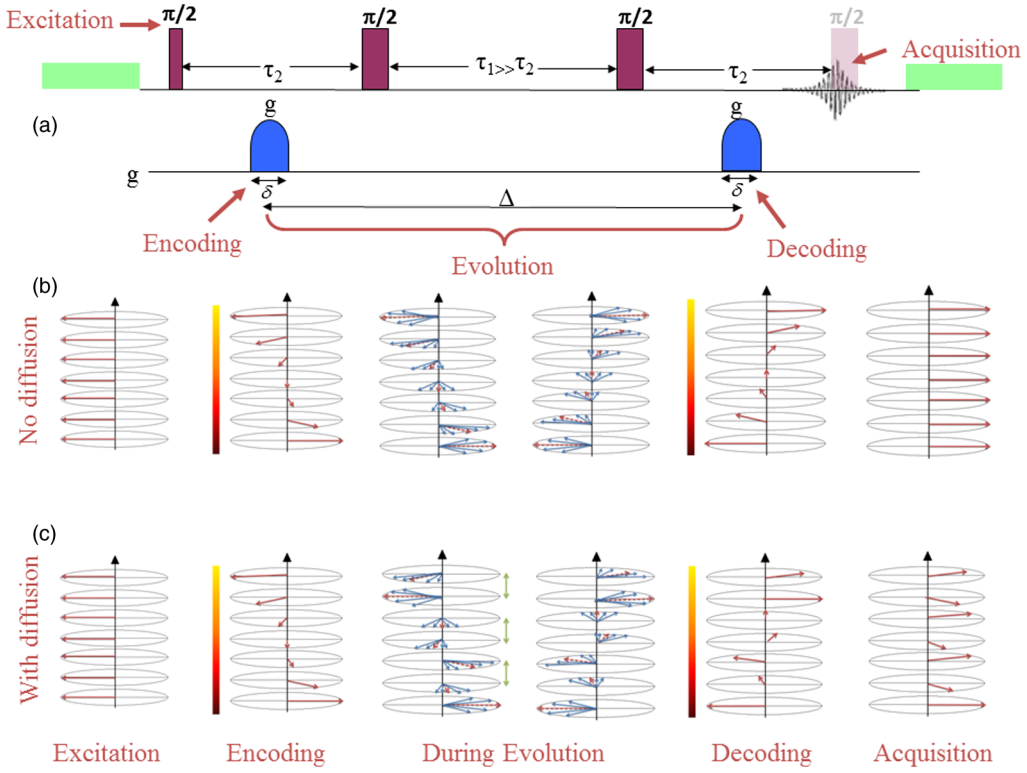

FIG. 3. (a) ESR pulse sequence for directly measuring the flip-flop rate through spin diffusion. The image depicts both the conventional induction-detection scheme as well as the optically detected scheme (with an additional $\pi/2$ MW pulse, shown in semitransparent mode, and the green laser irradiation before and after the sequence). (b),(c) Spin evolution can be described as follows: A $\pi/2$ excitation pulse creates magnetization along the $-x$ axis of the laboratory frame (the static field B_0 is along the z axis). A short magnetic-field gradient pulse creates variation in the Larmor precession frequencies. The result of this pulse is that the position of the spins along the field gradient is encoded in their phase. During the evolution time, spins can undergo a flip flop and thus distort the nicely ordered phase-encoded pattern (plate c, center). The two $\pi/2$ pulses applied during evolution just make sure that the phases are encoded along the z axis and thus stored for a period of T_1, typically much longer than T_2, to facilitate a relatively long evolution time. At the end of the evolution period, the spins are decoded with an identical short magnetic-field gradient pulse. If no diffusion occurred during the evolution period (plate b), the stimulated echo magnitude is maximal (affected only by T_1 and T_2 processes), while with flip-flop-mediated diffusion (plate c), refocusing is not complete and the echo signal is smaller. For optical detection, the MW sequence is preceded by a laser pulse that pumps the spin population of the NV triplet to its $m_s = 0$ state, and an additional MW pulse is applied to convert coherences to populations that affect the magnitude of the detected fluorescence signal [39].

magnitude of the flip-flop rate can be grossly estimated, to be [see Eq. (9)] $W \approx [\sqrt{2\pi}/(30T_2^{\mathrm{INT}})]$ [10,12]. This means that for a sample with approximately 10^{14} P atoms in 1 cm^3, where at approximately 4 K the value of T_2^{INT} is measured to be approximately 600 ms [15], $W \sim 0.03\ \mathrm{s}^{-1}$. The mean distance between like-electron spins (those that have the same quantum state for their neighboring nuclei) is $a \sim 270$ nm, which gives an estimated D_s of approximately $2.2 \times 10^{-15}\ \mathrm{m}^2/\mathrm{s}$ [Eq. (2)]. Similar arguments lead to $D_s \sim 3.1 \times 10^{-15}\ \mathrm{m}^2/\mathrm{s}$ for P concentrations of approximately 10^{-15}, based on T_2^{INT} data provided in Ref. [15], while for P concentrations of approximately 10^{16} atoms/cm^3 we can expect $D_s \sim 10^{-14}\ \mathrm{m}^2/\mathrm{s}$. These D_s values are extremely small and thus pose severe experimental challenges to measure them. More specifically, in order to be able to measure such diffusion effects, the term in the argument of the exponent in Eq. (10) involving D_s must be comparable to the terms with T_2 and T_1. As noted above, in recent years we have developed a methodology to measure the physical diffusion of electron spins in liquids. This capability relies on the use of a miniature resonator to acquire strong ESR signals from a very small sample, around which we place miniature gradient coils that make it possible to produce powerful magnetic-field gradients with a very short duration, as required by the PGSE sequence for electrons. Our latest achievements in this area allow us to obtain gradients of up to approximately 500 T/m with a pulse duration of approximately 1 μs [41]. Thus, even for a sample with approximately 10^{14} P atoms in 1 cm^3, it is possible, for example, to employ the sequence in Fig. 3 with values of τ_1 up to approximately $T_1/2 \sim 50$ ms (at 7 K [15,42]) and τ_2 of approximately 5 μs (to enable enough time to place in the gradient pulse—see Fig. 3). This implies that the factor $D_s\gamma^2 g^2 \delta^2(\Delta - \delta/3)$ can reach a value of approximately 0.8, while $2\tau_2/T_2 + \tau_1/T_1 \sim 0.5$, meaning that the expected echo decay due to spin diffusion should be considerable and measurable under such conditions. Similar arguments support also the experimental capability of measuring the diffusion of samples with higher P-atom concentrations at similar cryogenic temperatures.

IV. EXPERIMENTAL DETAILS

A. Samples

Two types of samples are employed in this study: (a) Phosphorus-doped ^{28}Si (^{28}Si:P) single crystal (^{28}Si purity of more than 99.9%) with a concentration of 10^{16} P atoms per cubic centimeter [43]. The doped isotopically enriched thin layer of 10-μm thickness is grown on a high-resistivity p-type silicon substrate [Fig. 4(a)]. At the measured temperature of 10 K, it is well known that such a sample behaves as an insulator with the electron spins fixed about the phosphorous nucleus [44–46]. (b) A synthetically grown diamond single crystal, type IIa, with a [111] face (purchased from Element Six, Germany), irradiated with 10-MeV electrons with a dose of $10^{18}\ \mathrm{cm}^{-2}$, resulting in NV concentrations of approximately 10^{14} spins/cm^3 (based on continuous-wave electron-spin-resonance measurements). These NVs are immobile at room temperature and the sample itself is highly insulated, precluding any real physical space electron motion. The diamond sample's dimensions are $3 \times 3 \times 0.34$ mm [see Fig. 4(b)].

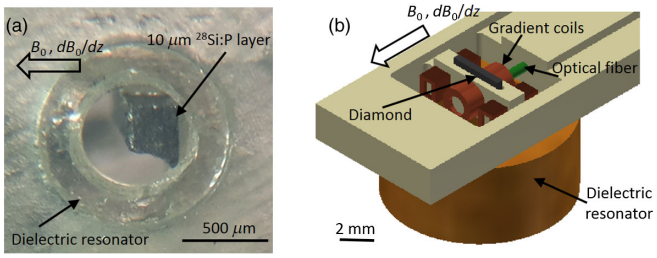

FIG. 4. The experimental setup for measuring the ^{28}Si:P sample (a) and the diamond sample (b).

B. Experimental system

The experiments are carried out employing our homemade pulsed ESR microimaging spectrometer as the main instrument console [47]. For the measurements of the ^{28}Si:P sample, we employ our cryogenic Q-band imaging probe head with a ring dielectric resonator [Fig. 4(a)], which is also equipped with a cryogenic low-noise amplifier for improved sensitivity [41,48]. The sample is placed with its plane perpendicular to the static field B_0, and the pulsed field gradients have a predominant dB_0/dz component [Fig. 4(a)]. The measurements of the diamond sample are carried out using our optically detected magnetic resonance imaging setup [49], but with a specially designed dielectric resonator for approximately 6.7 GHz, which can accommodate both the diamond sample and the gradient coils [Fig. 4(b)], for enhanced gradient efficiency (vs our setup in Ref. [49], where the gradient coils are outside rather than inside an approximately 10.6-GHz resonator). The sample is placed with its [111] orientation along B_0 to enable efficient optical pumping of the NV spins' levels. The gradient pulses are generated by our homemade half sine pulse drivers [33]. In the present experiments, we apply a gradient of 150 T/m for a duration δ of 1.1 μs for the ^{28}Si:P sample, while for the diamond sample gradients of 305 T/m are applied with a duration of $\delta = 550$ ns. The duration τ_2 is 25 μs for the ^{28}Si:P measurements and 8.3 μs for the NV sample. A 16-step phase-cycling scheme is used to cancel all unwanted FID and echo signals [50].

V. RESULTS AND DISCUSSION

A. Numerical simulation of the echo magnitude decay due to spin diffusion

The echo intensity measured with gradients, E^g, normalized to the echo intensity without gradients, E^0, when

using the pulse sequence shown in Fig. 3, can be directly linked to W via a numerical simulation that follows all the stages of the PGSE pulse sequence. The simulation takes a large number of electron spins (typically about 10 000) and places them randomly in a 3D space, with a mean distance that corresponds to their bulk concentration. Following this, the simulation applies a pulsed magnetic-field gradient that creates a corresponding spatially dependent phase profile for the spins in the sample along the z axis (parallel to the applied static field B_0). The spins are then given the opportunity to evolve during the evolution time with small time steps Δt (typically 100 μs). In terms of the simulation, this means that at each time step a given spin has a chance to flip flop with other spins. The flip-flop process between spins j and k, during a given short time step, is simulated as a random stochastic Markovian event with a probability of $\Delta t \times K_{ex}^2(3\cos^2\theta_{jk}-1)^2/r_{jk}^6$ [based on Eq. (8), with $K_{ex} \equiv \sqrt{(\pi/8)f_{jk}(0)}[(\mu_0/4\pi)\hbar\gamma_j\gamma_k]$]. Following the evolution time, the spins are then subjected to another gradient pulse that unwinds the phase profile generated by the first pulse. If no significant spin diffusion occurred via flip flops, the complex sum magnitude of all the spins in the sample should amount to their number. However, if many flip-flop events occurred, the complex sum becomes lower than the maximal value, as measured by our PGSE sequence. The only adjustable parameter in this numerical simulation is K_{ex} to fit the E^g/E^0 measured plot.

B. Spin diffusion in the ^{28}Si:P sample

ESR measurements with the pulse sequence shown in Fig. 3 are carried out at 8 K. The stimulated echo signal is recorded with and without the pulsed field gradients in an interleaved manner at a repetition rate of 10 Hz with evolution time ranging from 7 up to 60 ms (T_1 at this temperature is found to be approximately 30 ms). Measurements at each time point are averaged for a period of 1–5 min (longer averaging times for the longer evolution time where the echo signal is smaller). The echo signal with the pulsed field gradient, E^g, is normalized with respect to the echo signal without the phase gradients, E^0. Figure 5(a) shows the measured E^g/E^0 signal as a function of the evolution time. The figure also shows the theoretical fit, based on Eq. (10), normalized to E^0, i.e., $E^g/E^0 = \exp[-D_s\gamma^2 g^2\delta^2(\Delta-\delta/3)]$, with a single fit parameter $D_s = 3.37\times10^{-14}$ m^2/s, which translates through Eq. (2) to an exchange rate of $W \sim 15.9$ Hz (using $a \sim 46$ nm for P concentrations of $10^{16}/\text{cm}^3$). An additional fit is obtained by numerical simulation of the spin-diffusion phenomenon, which is more accurate than simply using Eq. (2) (see above), leading directly to a value of $K_{\text{ex}} = 1.2\times10^6$ [H$_z\times$nm^3], which for a distance of 46 nm and $\theta_{jk}=\pi/2$ gives $W\sim12.3$ Hz. The value of K_{ex} also provides information about the normalized zero quantum spectrum of the two-spin system [see Eq. (8)], to give $f_{jk}(0) = 3.8\times10^{-5}$ (for a spin distance of 46 nm).

C. Spin diffusion in the diamond sample

Similar stimulated echo measurements with and without the gradient pulses are carried out at room temperature on the diamond sample with the NV defects, but with the modified optically detected magnetic resonance (ODMR) PGSE sequence having two additional laser and one MW pulses (Fig. 3). As before, Fig. 5(b) shows the normalized echo signal E^g/E^0 as a function of the evolution time. However, due to the relatively short T_1 (approximately 5 ms) of the diamond sample at room temperature, we are limited to an evolution time of approximately 9 ms. In addition, it is evident that the error in these measurements is more prominent than in the first sample, and it is immediately noticeable that the normalized echo value starts from about 0.5 rather than from 1, even for a short evolution time. These issues are mainly due to three reasons: the relatively short T_2 of the diamond sample (approximately 10 μs) compared to that of the ^{28}Si:P (approximately 200 μs), its relatively large size (approximately 300 μm) compared to the thin (10 μm) enriched, layer of the Si sample, and the inherent problematics of the unique ODMR detection protocol.

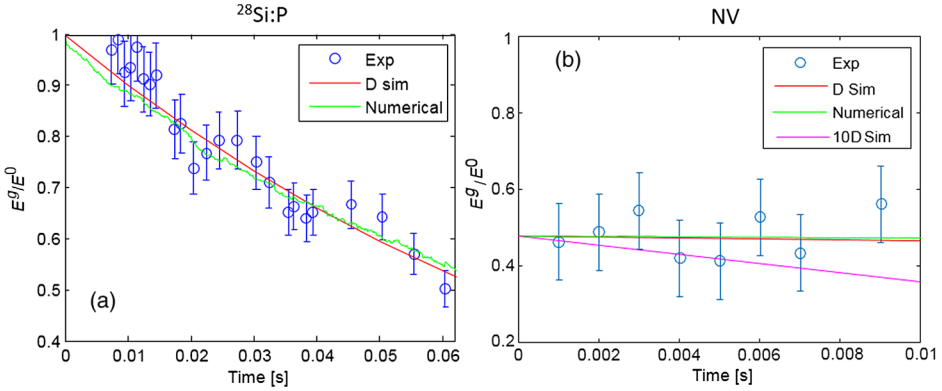

FIG. 5. (a) The ratio between the stimulated echo signal with pulse gradients, E^g, and the signal without pulse gradients, E^0, for the ^{28}Si:P sample. The fit to Eq. (10) is shown by the red line, and the numerical simulation results are shown by the green line. (b) The same as panel (a) but showing the measured and theoretical results for the sample of the NV centers in diamonds. An additional theoretical curve, assuming a tenfold larger spin-diffusion coefficient value, is shown in magenta (see the text for more explanations).

Let us explain what the implications of each of these three issues are. Pulsed magnetic-field gradients are never optimal, and residual small currents can persist in the gradient coils well after the pulse is applied. As noted above, since the gradient pulses can be applied only during the transverse evolution period, their duration should be comparable to or, better yet, much shorter than T_2. In the latter case, placing the gradient pulse at the beginning of the evolution period leaves enough time for the residual current to decay, during τ_2, which evidently cannot be much longer than T_2. In the ^{28}Si:P sample, due to its long T_2, we could employ a τ_2 of 25 μs, leaving more than enough time for the residual current to decay, while for the NV sample, with τ_2 of only 8.3 μs, some residual current apparently still remains. This residual current can shift the frequency of the echo signal and also broaden it. The shifting, and especially the broadening, effects greatly depend on the dimensions of the sample along the gradient axis. Here, also, the NV sample is inferior to the ^{28}Si:P, which is much thinner and thus much less prone to these artifacts. Finally, the ODMR detection protocol, with its need for an additional MW pulse to detect the echo signal, creates another problem. ODMR essentially collects the transverse magnetization echo signal at a single time point; therefore, any broadening or frequency shifts reduce the magnitude of the signal without any simple apparent way of restoring it. This is in contrast to the conventional induction-detection approach with quadrature detection, which collects the entire echo time evolution in a single acquisition. With induction detection, it is possible to immediately identify frequency changes and broadening effects that simply move and broaden the peak signal in the frequency spectrum domain. Thus, when such effects occur, they can be mostly reversed, and the undistorted total echo signal can be recovered by simply looking at the integral of the signal rather than at its maximum spectral value.

The above explanations and discussion make it clear why, at the high level of gradient pulses we employ, the normalized echo E^g/E^0 value shown in Fig. 5(b) already drops to a level of about 0.5, even for a very short evolution time. This is obviously not because of spin diffusion but rather due to the above-mentioned reasons, which limit the level of echo reconstruction that can be achieved with this sample in our present setup. Furthermore, as a result of the relatively short maximum evolution window and the large signal variability, we cannot observe a definite decay in the normalized echo signal. Nevertheless, while the signal and the corresponding results are far from optimal, it is still possible to draw some (albeit limited) physical conclusions based on it. For that purpose, we superimpose on the experimental data three theoretical decay curves. The first two are similar to those shown in Fig. 5(a), based on fitting the experimental data to the predictions of Eq. (10) and to the numerical simulation. With these two fits, we obtain a D_s value of approximately 1×10^{-14} m^2/s [fitting to Eq. (10)] and a K_{ex} value of approximately 2×10^6 H$_z$/nm^3, corresponding to $W \sim 0.2$ Hz (based on the numerical simulation results). The drop in the signal due to the effects of the residual current is accounted for by simply normalizing the simulation value to 0.47 instead of 1. Because of the quality of the data, these fitted values represent just a rough order of magnitude that provides an upper limit to the real physical values. To make this point clearer, a third theoretical plot is added, which represents the prediction of Eq. (10) but with a D_s value of approximately 1×10^{-13} m^2/s. This additional curve clearly shows that under our experimental conditions, for such a D_s value, the signal decay is expected to be much more pronounced, to a level that would have been measurable already during the 9-ms time slot. Thus, it can be concluded that the $W \sim 0.2$ Hz is indeed a rough order-of-magnitude upper limit to the flip-flop rate in this sample that can be estimated from our current experimental data.

The experimental results as a whole show the possibility to accurately measure the flip-flop rate of like-electron spins, as long as this rate is not much smaller than $1/T_1$. This condition is obeyed in the case of the ^{28}Si:P sample, but for the diamond sample this is not the case, and thus we can obtain only an upper limit for W. Our results can be compared to theory, based on Eq. (9), using the measured value for the intrinsic $T_2^{INT} \sim 1.05$ ms at 8 K for our ^{28}Si:P sample to obtain $W \sim 79.5$ Hz. In the case of the diamond sample, $T_2^{INT} \sim 90$ μs, leading to $W \sim 928$ Hz. These two theoretical rates are much faster than the measurements obtained by us. However, this is clearly due to the limitations of the simplified theory, because such fast rates are incompatible with our observations. In terms of a comparison to other experimental results, as noted above, such a type of measurements has not been carried out to date for electrons. The closest ones which are of relevance are the measurements carried out on a ^{28}Si:P sample with P concentrations of 10^{14} spins/cm^3 at 1.8 K, the findings of which are $T_2^{DFF} \sim 0.8$ s [15], corresponding to $W = 1/T_2^{DFF} \sim 1.25$ Hz [10]. The spin concentration in that case is 100 times lower than in our experiment, which suggests that W should also be much smaller (due to the dependence of the dipolar interaction on interspin distance). However, there should also be some temperature dependence affecting the entire process (via the spectral line width), and, thus, it is hard to conclude whether our results are in agreement with such a relaxation-time-based measurement or not.

VI. SUMMARY AND OUTLOOK

It can be concluded that the approach provided here for direct measurements of the flip-flop rate circumvents the difficulties associated with the extraction of this parameter using spin decoherence measurements. The acquisition of this rate is made possible thanks to advanced experimental capabilities in ESR that rely on high-sensitivity measurements

executed with fast and powerful pulsed field gradients. These can be applied to a variety of samples and should be an important characterization tool for various structures (vectors and 2D and 3D arrays) of spins, aiming at a variety of quantum-sensing and information-processing applications. Moreover, on a more basic level, these measurements open a window to address the issue of zero quantum spectral information (e.g., linewidth) in very weak electron-spin-coupled samples.

ACKNOWLEDGMENTS

This work is partially supported by Grant No. 310/13 from the Israel Science Foundation (ISF), Grant No. FA9550-13-1-0207 from the Air Force Office of Scientific Research (AFOSR), and Grant No. 3-12372 by the Israeli Ministry of Science.

[1] S. Steinert, F. Dolde, P. Neumann, A. Aird, B. Naydenov, G. Balasubramanian, F. Jelezko, and J. Wrachtrup, High sensitivity magnetic imaging using an array of spins in diamond, Rev. Sci. Instrum. **81**, 043705 (2010).
[2] C. Bonato, M. S. Blok, H. T. Dinani, D. W. Berry, M. L. Markham, D. J. Twitchen, and R. Hanson, Optimized quantum sensing with a single electron spin using real-time adaptive measurements, Nat. Nanotechnol. **11**, 247 (2016).
[3] J. J. L. Morton, D. R. McCamey, M. A. Eriksson, and S. A. Lyon, Embracing the quantum limit in silicon computing, Nature (London) **479**, 345 (2011).
[4] B. E. Kane, A silicon-based nuclear spin quantum computer, Nature (London) **393**, 133 (1998).
[5] W. Harneit, C. Meyer, A. Weidinger, D. Suter, and J. Twamley, Architectures for a spin quantum computer based on endohedral fullerenes, Phys. Status Solidi B **233**, 453 (2002).
[6] R. de Sousa, J. D. Delgado, and S. Das Sarma, Silicon quantum computation based on magnetic dipolar coupling, Phys. Rev. A **70**, 052304 (2004).
[7] L. C. L. Hollenberg, A. D. Greentree, A. G. Fowler, and C. J. Wellard, Two-dimensional architectures for donor-based quantum computing, Phys. Rev. B **74**, 045311 (2006).
[8] N. Y. Yao, L. Jiang, A. V. Gorshkov, P. C. Maurer, G. Giedke, J. I. Cirac, and M. D. Lukin, Scalable architecture for a room temperature solid-state quantum information processor, Nat. Commun. **3**, 800 (2012).
[9] V. V. Kurshev and T. Ichikawa, Effect of spin flip-flop on electron-spin-echo decay due to instantaneous diffusion, J. Magn. Reson. **96**, 563 (1992).
[10] N. Bloembergen, On the interaction of nuclear spins in a crystalline lattice, Physica (Amsterdam) **15**, 386 (1949).
[11] I. M. Nolden and R. J. Silbey, Simulation of spin diffusion in a disordered system, Phys. Rev. B **54**, 381 (1996).
[12] A. Abragam, *The Principles of Nuclear Magnetism* (Clarendon, Oxford, 1961).
[13] M. Ernst and B. Meier, in *Studies in Physical and theoretical chemistry Solid State NMR of Polymers* (Elsevier, New York, 1998), p. 83.
[14] J. Dolinsek, P. M. Cereghetti, and R. Kind, Phonon-assisted spin diffusion in solids, J. Magn. Reson. **146**, 335 (2000).
[15] A. M. Tyryshkin, S. Tojo, J. J. L. Morton, H. Riemann, N. V. Abrosimov, P. Becker, H. J. Pohl, T. Schenkel, M. L. W. Thewalt, K. M. Itoh, and S. A. Lyon, Electron spin coherence exceeding seconds in high-purity silicon, Nat. Mater. **11**, 143 (2012).
[16] E. L. Hahn, Spin echoes, Phys. Rev. **80**, 580 (1950).
[17] H. Y. Carr and E. M. Purcell, Effects of diffusion on free precession in nuclear magnetic-resonance experiments, Phys. Rev. **94**, 630 (1954).
[18] W. M. Witzel, M. S. Carroll, A. Morello, L. Cywinski, and S. Das Sarma, Electron Spin Decoherence in Isotope-Enriched Silicon, Phys. Rev. Lett. **105**, 187602 (2010).
[19] A. Blank, Scheme for a spin-based quantum computer employing induction detection and imaging, Quantum Inf. Process. **12**, 2993 (2013).
[20] S. Prawer and I. Aharonovich, *Quantum Information Processing with Diamond* (Woodhead Publishing, Cambridge, 2014).
[21] D. Suter and R. R. Ernst, Spin diffusion in resolved solid-state NMR-spectra, Phys. Rev. B **32**, 5608 (1985).
[22] C. G. Tang and J. S. Waugh, Dynamics of classical spins on a lattice—Spin diffusion, Phys. Rev. B **45**, 748 (1992).
[23] E. O. Stejskal and J. E. Tanner, Spin diffusion measurements—Spin echoes in presence of a time-dependent field gradient, J. Chem. Phys. **42**, 288 (1965).
[24] P. T. Callaghan, A. Coy, D. Macgowan, K. J. Packer, and F. O. Zelaya, Diffraction-like effects in NMR diffusion studies of fluids in porous solids, Nature (London) **351**, 467 (1991).
[25] P. T. Callaghan, *Translational Dynamics and Magnetic Resonance: Principles of Pulsed Gradient Spin Echo NMR* (Oxford University Press, New York, 2011).
[26] H. A. Reich, Nuclear magnetic resonance in solid Helium-3, Phys. Rev. **129**, 630 (1963).
[27] J. R. Thompson, E. R. Hunt, and H. Meyer, Spin diffusion in solid ^{3}He, Phys. Lett. **25A**, 313 (1967).
[28] W. R. Zhang and D. G. Cory, First Direct Measurement of the Spin Diffusion Rate in a Homogenous Solid, Phys. Rev. Lett. **80**, 1324 (1998).
[29] K. W. Eberhardt, S. Mouaziz, G. Boero, J. Brugger, and B. H. Meier, Direct Observation of Nuclear Spin Diffusion in Real Space, Phys. Rev. Lett. **99**, 227603 (2007).
[30] G. G. Maresch, A. Grupp, M. Mehring, J. U. Vonschutz, and H. C. Wolf, Direct observation of one-dimensional electron-spin transport in the organic conductor (Fa)2asf6 by the electron-spin echo field gradient technique, J. Phys. (Paris) **46**, 461 (1985).
[31] Y. Talmon, L. Shtirberg, W. Harneit, O. Y. Rogozhnikova, V. Tormyshev, and A. Blank, Molecular diffusion in porous media by PGSE ESR, Phys. Chem. Chem. Phys. **12**, 5998 (2010).
[32] A. Blank, Y. Talmon, M. Shklyar, L. Shtirberg, and W. Harneit, Direct measurement of diffusion in liquid phase by electron spin resonance, Chem. Phys. Lett. **465**, 147 (2008).
[33] L. Shtirberg and A. Blank, Short, powerful, and agile current drivers for magnetic resonance, Concepts Magn. Reson., Part B **39B**, 119 (2011).

[34] S. P. Dash, S. Sharma, R. S. Patel, M. P. de Jong, and R. Jansen, Electrical creation of spin polarization in silicon at room temperature, Nature (London) **462**, 491 (2009).

[35] M. Furis, D. L. Smith, S. Kos, E. S. Garlid, K. S. M. Reddy, C. J. Palmstrom, P. A. Crowell, and S. A. Crooker, Local Hanle-effect studies of spin drift and diffusion in n: GaAs epilayers and spin-transport devices, New J. Phys. **9**, 347 (2007).

[36] A. J. Drew, J. Hoppler, L. Schulz, F. L. Pratt, P. Desai, P. Shakya, T. Kreouzis, W. P. Gillin, A. Suter, N. A. Morley, V. K. Malik, A. Dubroka, K. W. Kim, H. Bouyanfif, F. Bourqui, C. Bernhard, R. Scheuermann, G. J. Nieuwenhuys, T. Prokscha, and E. Morenzoni, Direct measurement of the electronic spin diffusion length in a fully functional organic spin valve by low-energy muon spin rotation, Nat. Mater. **8**, 109 (2009).

[37] V. M. Axt and T. Kuhn, Femtosecond spectroscopy in semiconductors: A key to coherences, correlations and quantum kinetics, Rep. Prog. Phys. **67**, 433 (2004).

[38] B. A. Ruzicka, L. K. Werake, H. Samassekou, and H. Zhao, Ambipolar diffusion of photoexcited carriers in bulk GaAs, Appl. Phys. Lett. **97**, 262119 (2010).

[39] E. Vanoort, N. B. Manson, and M. Glasbeek, Optically detected spin coherence of the diamond N-V center in its triplet ground-state, J. Phys. C **21**, 4385 (1988).

[40] J. E. Tanner, Use of stimulated echo in NMR-diffusion studies, J. Chem. Phys. **52**, 2523 (1970).

[41] Y. Artzi, Y. Twig, and A. Blank, Induction-detection electron spin resonance with spin sensitivity of a few tens of spins, Appl. Phys. Lett. **106**, 084104 (2015).

[42] A. M. Tyryshkin, S. A. Lyon, A. V. Astashkin, and A. M. Raitsimring, Electron spin relaxation times of phosphorus donors in silicon, Phys. Rev. B **68**, 193207 (2003).

[43] Y. Twig, E. Dikarov, W. D. Hutchison, and A. Blank, Note: High sensitivity pulsed electron spin resonance spectroscopy with induction detection, Rev. Sci. Instrum. **82**, 076105 (2011).

[44] K. Sumida, K. Ninomiya, M. Fujii, K. Fujio, S. Hayashi, M. Kodama, and H. Ohta, Electron spin-resonance studies of conduction electrons in phosphorus-doped silicon nanocrystals, J. Appl. Phys. **101**, 033504 (2007).

[45] G. Feher, Electron spin resonance experiments on donors in silicon. I. electronic structure of donors by the electron nuclear double resonance technique, Phys. Rev. **114**, 1219 (1959).

[46] C. F. Young, E. H. Poindexter, G. J. Gerardi, W. L. Warren, and D. J. Keeble, Electron paramagnetic resonance of conduction-band electrons in silicon, Phys. Rev. B **55**, 16245 (1997).

[47] L. Shtirberg, Y. Twig, E. Dikarov, R. Halevy, M. Levit, and A. Blank, High-sensitivity Q-band electron spin resonance imaging system with submicron resolution, Rev. Sci. Instrum. **82**, 043708 (2011).

[48] Y. Twig, E. Dikarov, and A. Blank, Cryogenic electron spin resonance microimaging probe, J. Magn. Reson. **218**, 22 (2012).

[49] A. Blank, G. Shapiro, R. Fischer, P. London, and D. Gershoni, Optically detected magnetic resonance imaging, Appl. Phys. Lett. **106**, 034102 (2015).

[50] A. Schweiger and G. Jeschke, *Principles of Pulse Electron Paramagnetic Resonance* (Oxford University, New York, 2001).